Tenth International Conference on Computational Fluid Dynamics (ICCFD10), Barcelona,Spain, July 9-13, 2018 **ICCFD10-2018-0167**

Simulations of Shallow Water Surface Waves and Comparison with Water Table Experiments

M. Hafez, A. Chuen and A. Burkhead, University of California, Davis (UCD)
Dedicated to the memory of Dr. Meng-Sing Liou of NASA Glenn

Abstract: The hyperbolic systems of equations describing the shallow water surface waves are solved numerically using finite difference schemes and an explicit time integration procedure. The equations are similar to Isentropic Euler equations (with $\gamma = 2$) and can be simplified using a potential flow model. The results of Isentropic Euler, potential model and full Euler equations are compared for typical flows around pointed and blunt bodies for several Mach numbers. On the other hand, water table experiments are described and the flow over obstacles are studied. Using the theory of Hydraulic Analogy, the relations between compressible flows and shallow water surface waves are discussed. Flow patterns, including formation of shock waves and expansion fans are presented. It is demonstrated that the water table can be an inexpensive educational tool for demonstration of transonic and supersonic flow phenomena.

1 Introduction

Supersonic wind tunnels are very expensive. To show students shock waves, one can use instead a water table experiment. The purpose of this work is to exploit the relation between compressible flows and shallow water surface waves to demonstrate, in the classroom, the details of flow patterns around different shapes. Numerical simulations, with a simple code, should produce similar results, at least qualitatively. The governing equations for the shallow water surface waves, assuming hydrostatic pressure across the layer, are derived, see ref [1, 2, 3]. The governing equations for one dimensional flows in a variable area duct are also given.

Next, the two dimensional compressible flow equations are considered, including the full Euler Equations, the Isentropic Euler Equations, the full Potential Equation, and the Transonic Small Disturbance approximation. The analogy between shallow water waves and the two dimensional compressible flow is then established and the limitations are outlined.

Numerical simulations based on the equations in conservation forms augmented with artificial viscosity terms are discussed. More sophisticated schemes are given in ref [1, 2]. The theory of hydraulic analogy is described in ref [3, 4], while the water table experiment is discussed in ref [5]. Typical numerical and experimental results are shown for a cylindrical and diamond airfoil, as well as for internal flows in nozzles. Finally, some concluding remarks are mentioned.

2 Governing Equations

The equations governing shallow water surface waves are

$$(\rho_w h)_t + (\rho_w u h)_x + (\rho_w v h)_y = 0 \tag{1}$$

$$\rho_w u_t + \rho_w u u_x + \rho_w v u_y = -P_x \tag{2}$$

$$\rho_w v_t + \rho_w u v_x + \rho_w v v_y = -P_y \tag{3}$$

where,

$$P = P_{atm} + \rho_w g(h - z).$$

Hence,

$$P_x = \rho_w g h_x P_y = \rho_w g h_y$$

Notice ρ_w drops off all of the equations. The momentum equation can be rewritten in conservation form as follows.

$$(hu)_t + (hu^2)_x + (huv)_y = -\frac{1}{2}g(h^2)_x \tag{4}$$

$$(hv)_t + (huv)_x + (hv^2)_y = -\frac{1}{2}g(h^2)_y \tag{5}$$

These can be represented in the non dimensional form:

$$(hu)_t + (hu^2)_x + (huv)_y = -\frac{1}{2}\frac{1}{Fr}(h^2)_x \tag{6}$$

$$(hv)_t + (huv)_x + (hv^2)_y = -\frac{1}{2}\frac{1}{Fr}(h^2)_y \tag{7}$$

Where h is now normalized by h_∞ and u, v are normalized by V_∞. The Froude number (Fr) is given by $Fr = \frac{V_\infty}{gh_\infty}$, where $gh_\infty = c_\infty^2$ and c_∞ is the speed of surface waves far from the body.
The governing equations for unsteady two dimensional compressible flows are as follows.

$$\rho_t + (\rho u)_x + (\rho v)_y = 0 \tag{8}$$

$$(\rho u)_t + (\rho u^2)_x + (\rho uv)_y = -P_x \tag{9}$$

$$(\rho v)_t + (\rho uv)_x + (\rho v^2)_y = -P_y \tag{10}$$

$$(\rho E)_t + (\rho uH)_x + (\rho vH)_y = 0 \tag{11}$$

Where E is the internal energy, H is the total enthalpy, and $H = E + \frac{P}{\rho} = c_v T + \frac{P}{\rho} + \frac{1}{2}(u^2 + v^2)$, ignoring the potential energy terms.
The isentropic Euler equations, in non dimensional form are shown below.

$$\rho_t + (\rho u)_x + (\rho v)_y = 0 \tag{12}$$

$$(\rho u)_t + (\rho u^2)_x + (\rho uv)_y = -P_x \tag{13}$$

$$(\rho v)_t + (\rho uv)_x + (\rho v^2)_y = -P_y \tag{14}$$

Where the pressure is normalized by $\rho_\infty V_\infty^2$ and the isentropic relation is $P = \frac{\rho^\gamma}{\gamma M_\infty^2}$
A potential flow model can be used where:

$$\rho_t + (\rho\Phi_x)_x + (\rho\Phi_y)_y = 0 \tag{15}$$

$$\Phi_t + \frac{\rho^\gamma - 1}{(\gamma - 1)M_\infty^2} + \frac{1}{2}((\nabla\Phi)^2 - 1) = 0 \tag{16}$$

The second equation is Bernoulli's law for unsteady flows, with no time variation in the far field.
The Transonic Small Disturbance approximation is given as:

$$u_t = ((1 - M_\infty^2)u - \frac{1}{2}(\gamma + 1)M_\infty^2 u^2)_x + v_y \tag{17}$$

$$\beta v_t = -v_x + u_y \tag{18}$$

Where u, v are the perturbation velocity components. For $\beta = 0$, the second equation represents the irrotationality condition. We used $\beta = 1$ and the system becomes symmetric hyperbolic equations. Together with the no-penetration boundary condition at solid surfaces and vanishing disturbances in the far-field, the above formulations are complete.

For simplicity, the Hydraulic Analogy is outlined, for the case of steady quasi-one dimensional nozzle flow, in Figure 1.

The density of compressible flow corresponds to the height of the thin water layer over a flat plate, and the Mach number corresponds to the Froude number. The limitations of the analogy are clear. The flow is assumed isentropic and the ratio of specific heats, $\gamma = 2$.

The governing equations for steady flow in a nozzle are the conservation laws of mass, momentum, and energy. The law for mass conservation and that for momentum conservation can be combined in the form:

$$(u + \bar{P})_x = -\frac{A_x}{A}\bar{P} \tag{19}$$

Where u is normalized by a^*, the speed of sound at sonic conditions, and A is normalized by A^*, the throat area. Notice that $\bar{P} = AP$, and the expression $\bar{P} = (\frac{\gamma+1}{2\gamma})\frac{1}{u} - (\frac{\gamma-1}{2\gamma})u$ can be derived taking the total enthalpy as constant. For smooth flows, this equation can be integrated to give a standard relation for $\frac{A}{A^*}$ as a function of M^*. For a given value of $\frac{A}{A^*}$, there are two solutions, one with $M^* < 1$ and the other with $M^* > 1$. For flow with a shock, the jump condition across the shock is $M_1^* M_2^* = 1$

On the other hand, for isentropic Euler, the pressure is related to density by $P = \frac{1}{\gamma}\rho^\gamma$. For the case of $\gamma = 2$, $\bar{P} = \frac{1}{2}\frac{A}{(Au)^2}$. The smooth solution is the same as the full Euler case, but for solutions with shocks, the shock jump conditions are different.

3 Numerical Methods

We present two methods for steady quasi one dimensional flows in nozzles, shock fitting and upwind scheme, for both the full and isentropic Euler formulations. To simulate flow with a shock, we calculate two branches of the solution in the divergent part of a convergent/divergent nozzle. One starts from the throat, marching point by point in space, to the exit using second order accurate discretization and Newton's iteration at each step to account for non-linearity. Similarly, the second branch is calculated by starting at the exit and marching backwards. The shock is located by joining the two branches at a point, where the shock jump condition $(u + P)_1 = (u + P)_2$ is satisfied, or $M_1^* M_2^* = 1$ for full Euler.

The upwind scheme is based on forward and backward calculations as before, except an artificial viscosity in conservation form is added to capture the shock. Uniform artificial viscosity of the order Δx, will smear the shock profile. On the other hand, using a variable viscosity coefficient leads to a sharper shock. The viscosity coefficient is chosen to be proportional to

$$\nu_{i+\frac{1}{2}} = \alpha\frac{|u_{i+1} - u_i|^2}{|u_{i+1}|^2 + |u_i|^2}, \quad \nu_{i-\frac{1}{2}} = \alpha\frac{|u_i - u_{i-1}|^2}{|u_i|^2 + |u_{i-1}|^2} \tag{20}$$

The numerical results for full and isentropic Euler calculations for a simple converging-diverging nozzle are shown in Figures 2, 3. The full Euler calculations are in good agreement with the results of [6].

Calculations for nozzles with two throats are shown in Figures 4, 5. Results for three throats are presented in Figures 6, and 7. The results are in good agreement with the results of [7], where non-unique solutions are reported for these nozzle geometries.

On the other hand, a more general scheme is used, with marching in time, not in space. Consider the one dimensional example:

$$u_t + uu_x = (\epsilon u_x)_x \tag{21}$$

Where ϵ is the coefficient of artificial viscosity. With the boundary conditions $u(-1) = 1$, $u(1) = -1$ and $u(x, 0) = sin(n\pi x) + c$ the equation is augmented with a second order term with derivatives in time. The modified equation reads

$$\beta u_{tt} + u_t + \frac{1}{2}(u^2)_x = (\epsilon u_x)_x. \tag{22}$$

Central differences are used in time and in space to construct an explicit, three-level scheme. The coefficient β is chosen to guarantee numerical stability. In the present case, β is of order unity.

$$\beta_{i,n}\frac{u_{i,n+1}-2u_{i,n}+u_{i,n-1}}{\Delta t^2}+\frac{u_{i,n+1}-u_{i,n-1}}{2\Delta t}+\frac{\frac{1}{2}(u^2_{i+1,n}-u^2_{i-1,n})}{2\Delta x}=$$
$$\frac{1}{\Delta x}[\epsilon_{i+\frac{1}{2},n}\frac{u_{i+1,n}-u_{i,n}}{\Delta x}-\epsilon_{i-\frac{1}{2},n}\frac{u_{i,n}-u_{i-1,n}}{\Delta x}]. \quad (23)$$

Figure 8 shows the initial condition and the final solution. As expected, the final solution exhibits a shock in the middle of the domain with only some slight smearing over several points. Numerical results for nozzle flows are shown in Figures 9, 10, and 11,

To apply the above scheme to systems of two or three equations for two dimensional flows, we use:

$$\beta\vec{W}_{tt}+\vec{W}_t+\vec{F}\left(\vec{W}\right)_x+\vec{G}\left(\vec{W}\right)_y=\left(\epsilon_1\vec{W}_x\right)_x+\left(\epsilon_2\vec{W}_y\right)_y \quad (24)$$

Again, central differences are used in time and in space to construct an explicit three level scheme. The convergence to steady state can be accelerated as will be described somewhere else. A fourth-order artificial viscosity proportional to $\nabla^2\epsilon_0\nabla^2\vec{W}$ can be blended with the above second order terms if higher order accuracy is required.

The numerical results for the flow over a wavy wall are shown in Figure 12. Numerical results for supersonic flow around a cylinder at Mach 1.2 and 1.4 are presented in Figures 13 and 14. These solutions were obtained by solving the isentropic Euler equations ($\gamma = 2$) using the scheme presented in equation 24 over a polar coordinate grid.

Numerical results for transonic and supersonic over a diamond airfoil at Mach numbers $0.85, 0.95, 1.1$, and 1.4 are presented in Figures 15, 16, 17, and 18, respectively. Each set of figures present similar solutions computed using the different fluid equations presented in Section 2. The dissipation scheme from equation 24 are also utilized for shock capturing.

4 Experimental Results

Experiments are run on a table built at UCD, shown in Figure 19 , in order to observe the analogous shock patterns. The water table allows for models of various geometry to be attached to a 1.6 meter long motorized track. The maximum speed of the track is 0.698 meters per second. Figure 20a and Figure 20b display both a detached bow shock in front of a cylinder model and an attached oblique shock on a diamond airfoil.

Flow over a wavy wall is shown in Figure 21a and flow over a concave wall is shown in Figure 21b . Flow over a cylinder with (a two dimensional) spike is shown in Figure 21c . Notice the formation of the attached shock because of the spike, followed by the curved shock. Flow through a converging-diverging, double, and triple nozzle are shown in Figures 22, 23, and 24, respectively.

5 Concluding Remarks

Numerical simulations of shallow water surface waves are presented using an explicit three level scheme for several models. Qualitative comparisons with experimental results of water table experiments are encouraging. More work is needed to demonstrate quantitatively the validity of the hydraulic analogy, in particular for cases with unsteady flows.

6 Acknowledgements

This work is funded by the NSF Improving Undergraduate STEM Education (IUSE) Program Award No. 1505080.

References

[1] Eleuterio Francisco Toro. *Shock-Capturing Methods for Free-Surface Shallow Flows.* Wiley and Sons Ltd., 2001.

[2] W. Y. Tan. *Shallow Water Hydrodynamics: Mathematical Theory and Numerical Solution for a Two-dimensional System of Shallow-water Equations.* Elsevier, August 1992.

[3] J. J. Chattot and M. M. Hafez. *Theoretical and Applied Aerodynamics.* Springer Netherlands, Dordrecht, 2015.

[4] M. Hafez. Hydraulic analogy and visualisation of two-dimensional compressible fluid flows: part 1: theoretical aspects. *International Journal of Aerodynamics*, 6(1):41–66, January 2018.

[5] M. Hafez, F. Jan, B. Linke, and I. Garretson. Hydraulic analogy and visualisation of two-dimensional compressible fluid flows: part 2: water table experiments. *International Journal of Aerodynamics*, 6(1):67–82, January 2018.

[6] Jean-Jacques Chattot. *Computational Aerodynamics and Fluid Dynamics: An Introduction.* Springer Science & Business Media, February 2004.

[7] Pavel Solin and Karel Segeth. Non-Uniqueness of Almost Unidirectional Inviscid Compressible Flow. *Applications of Mathematics*, 49(3):247–268, June 2004.

Hydraulic Analogy

2D Compressible Fluid Flow

$$\rho u A = \rho_r u_r A_r = \text{constant}$$

$$\frac{\rho}{\rho_r} \cdot \frac{u}{u_r} \cdot \frac{A}{A_r} = 1$$

$$\rho u \frac{du}{dx} = -\frac{dP}{dx} = \frac{dP}{d\rho} \cdot \frac{d\rho}{dx}$$

$$\frac{dP}{d\rho} = a^2 \rightarrow \quad u\frac{du}{dx} = -\frac{a^2}{\rho} \cdot \frac{d\rho}{dx}$$

$$a^2 = \frac{dP}{d\rho} = \frac{\gamma P}{\rho} = \gamma R T$$

$$\frac{P}{P_r} = \left(\frac{\rho}{\rho_r}\right)^{\gamma} = \left(\frac{T}{T_r}\right)^{\frac{\gamma}{\gamma - 1}}$$

Poisson's Adiabatic

$$\frac{a^2}{a_\infty^2} = \frac{\gamma R T}{\gamma R T_\infty} = \frac{T}{T_\infty}$$

$$\frac{u}{u_\infty} \cdot \frac{d\left(\frac{u}{u_\infty}\right)}{dx} = -\frac{a^2}{a_\infty^2} \cdot \frac{a_\infty^2}{u_\infty^2} \cdot \frac{\frac{d\left(\rho/\rho_\infty\right)}{dx}}{\rho/\rho_\infty}$$

Shallow Water Surface Wave

$$\rho_w h u A = \rho_w h_r u_r A_r$$

$$\frac{h}{h_r} \cdot \frac{u}{u_r} \cdot \frac{A}{A_r} = 1$$

$$\rho_w u \frac{du}{dx} = -\frac{dP}{dx}$$

Hydrostatic Equation

$$P = P_{atm} + \rho_w g (h - z)$$

$$\frac{dP}{dx} = \rho_w g \frac{dh}{dx}$$

$$\rho_w u \frac{du}{dx} = -\rho_w g \frac{dh}{dx}$$

$$u\frac{du}{dx} = -\frac{gh\frac{dh}{dx}}{h}$$

Speed of Surface Wave

$$c = \sqrt{gh}$$

$$\frac{u}{u_\infty} \cdot \frac{d\left(\frac{u}{u_\infty}\right)}{dx} = -\frac{gh}{gh_\infty} \cdot \frac{gh_\infty}{u_\infty^2} \cdot \frac{\frac{d\left(h/h_\infty\right)}{dx}}{h/h_\infty}$$

Analogy

$$\frac{\rho}{\rho_\infty} = \frac{h}{h_\infty} \quad , \quad \frac{a^2}{a_\infty^2} = \frac{gh}{gh_\infty} = \frac{T}{T_\infty}$$

$$\frac{P}{P_\infty} = \frac{\rho R T}{\rho_\infty R T_\infty} = \frac{\rho}{\rho_\infty} \cdot \frac{T}{T_\infty} = \left(\frac{h}{h_\infty}\right)^2 \qquad \gamma = 2$$

Mach Number vs Froud Number

$$M_a^2 = \frac{u_\infty^2}{a_\infty^2} \qquad F_r^2 = \frac{u_\infty^2}{gh_\infty}$$

Figure 1: Quasi one dimensional hydraulic analogy summary.

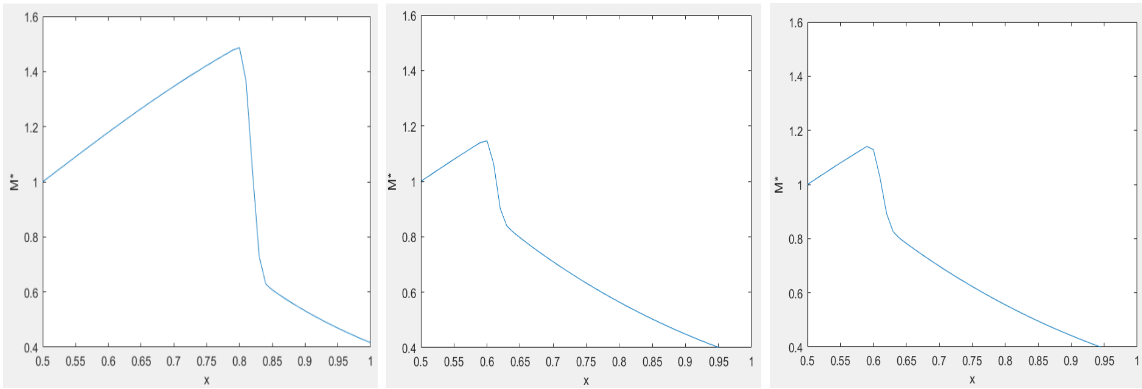

(a) Full Euler $\gamma = 1.4$ (b) Full Euler $\gamma = 2$ (c) Isentropic Euler $\gamma = 2$

Figure 2: Upwind scheme results, showing M^* for simple converging-diverging nozzle

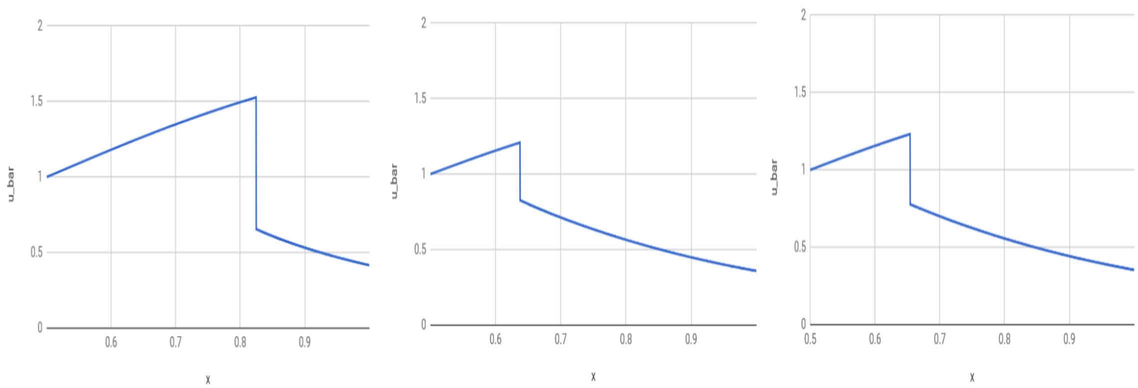

(a) Full Euler $\gamma = 1.4$ (b) Full Euler $\gamma = 2$ (c) Isentropic Euler $\gamma = 2$

Figure 3: Shock fitting results, showing M^* for simple converging-diverging nozzle

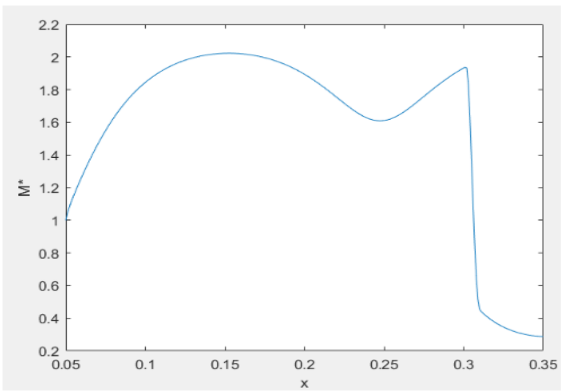

(a) Full Euler $\gamma = 1.4$ (1 shock)

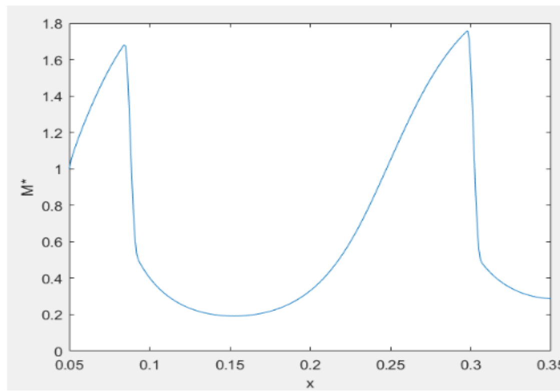

(b) Full Euler $\gamma = 1.4$ (2 shocks)

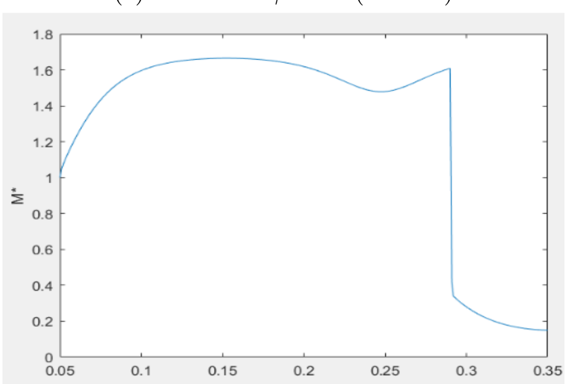

(c) Isentropic Euler $\gamma = 2$ (1 shock)

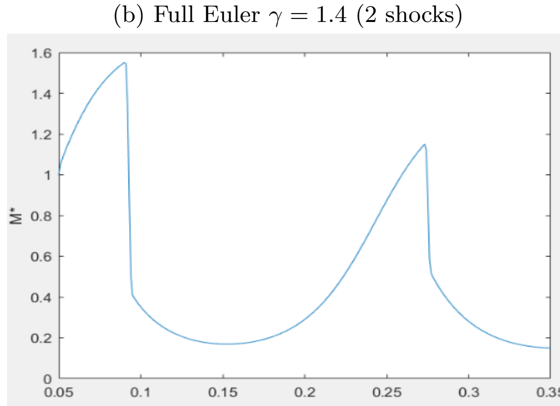

(d) Isentropic Euler $\gamma = 2$ (2 shocks)

Figure 4: Upwind scheme results, showing M^* for the double throat nozzle

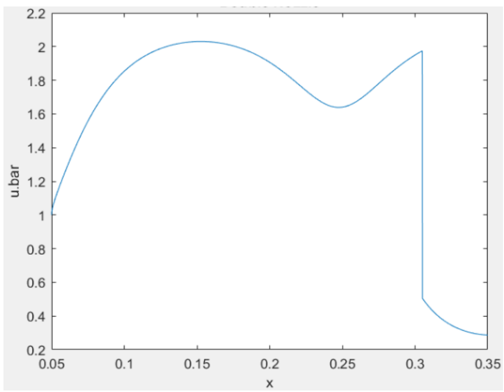

(a) Full Euler $\gamma = 1.4$

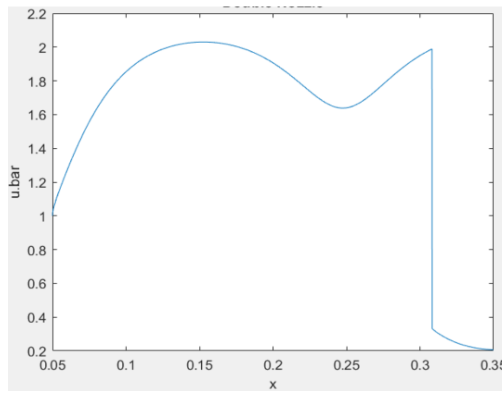

(b) Isentropic Euler $\gamma = 1.4$

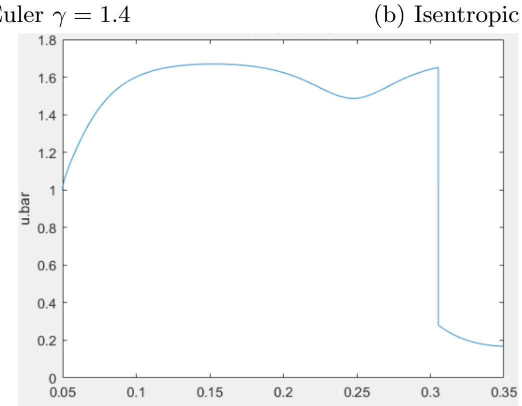

(c) Isentropic Euler $\gamma = 2$

Figure 5: Shock fitting results, showing M^* for the double throat nozzle

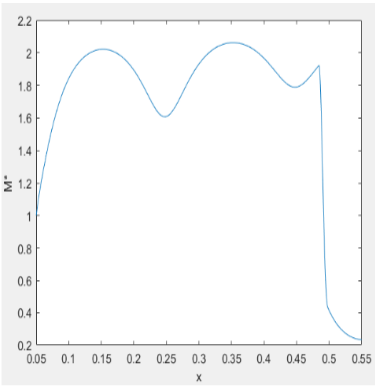

(a) Full Euler $\gamma = 1.4$ (1 shock)

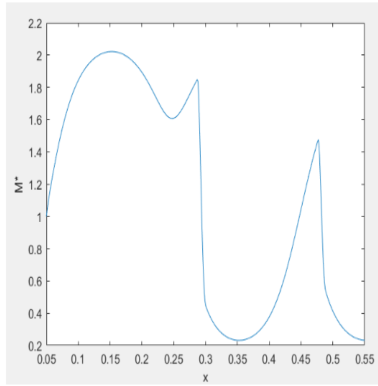

(b) Full Euler $\gamma = 1.4$ (2 shocks)

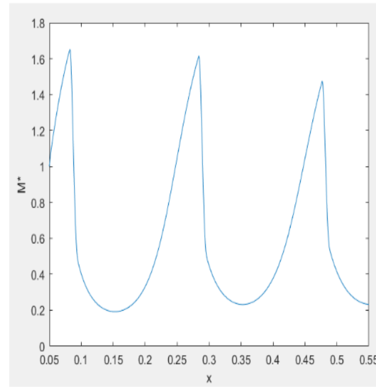

(c) Full Euler $\gamma = 1.4$ (3 shocks)

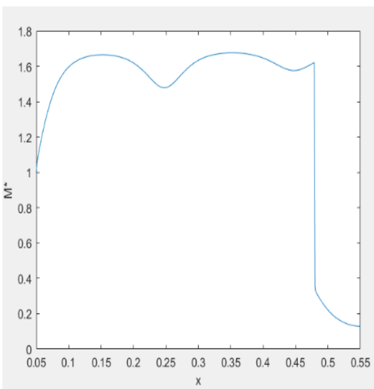

(d) Isent. Euler $\gamma = 2$ (1 shock)

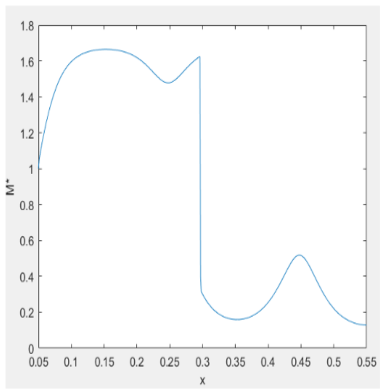

(e) Isent. Euler $\gamma = 2$ (2 shocks)

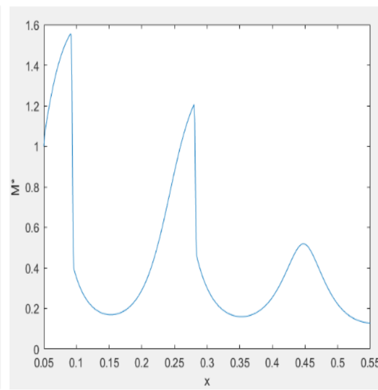

(f) Isent. Euler $\gamma = 2$ (3 shocks)

Figure 6: Upwind scheme results, showing M^* for the triple throat nozzle

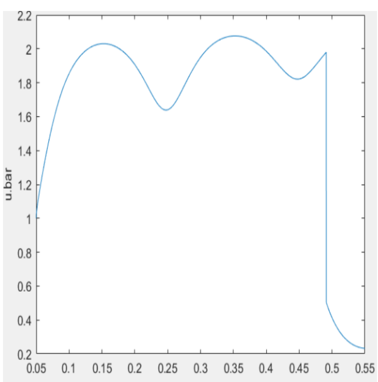

(a) Full Euler $\gamma = 1.4$

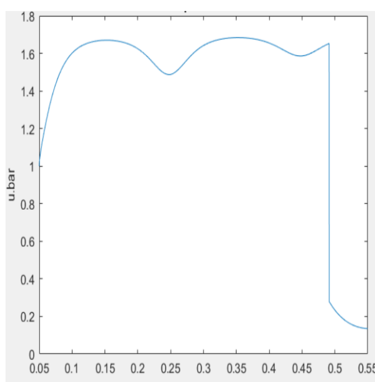

(b) Isentropic Euler $\gamma = 1.4$

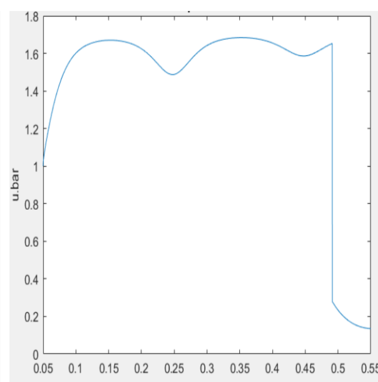

(c) Isentropic Euler $\gamma = 2$

Figure 7: Shock fitting results, showing M^* for the triple throat nozzle

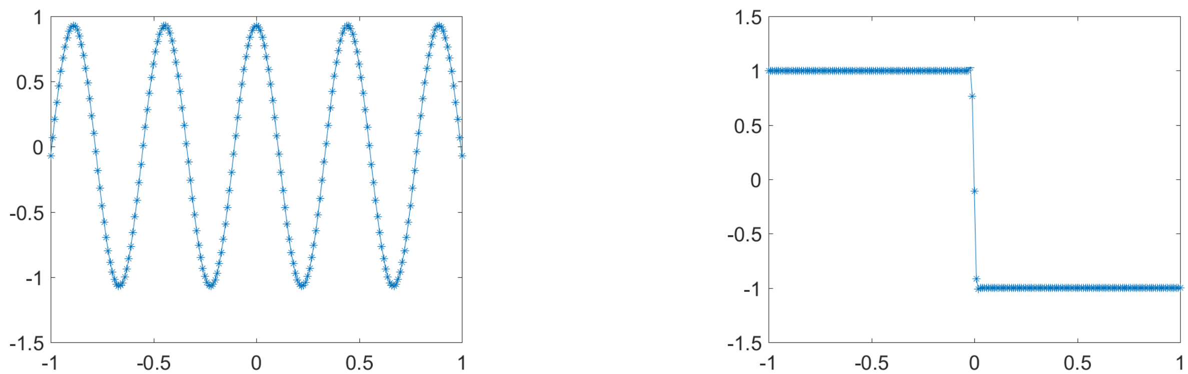

(a) Initial condition. (b) Solution.

Figure 8: Simple scalar transport problem.

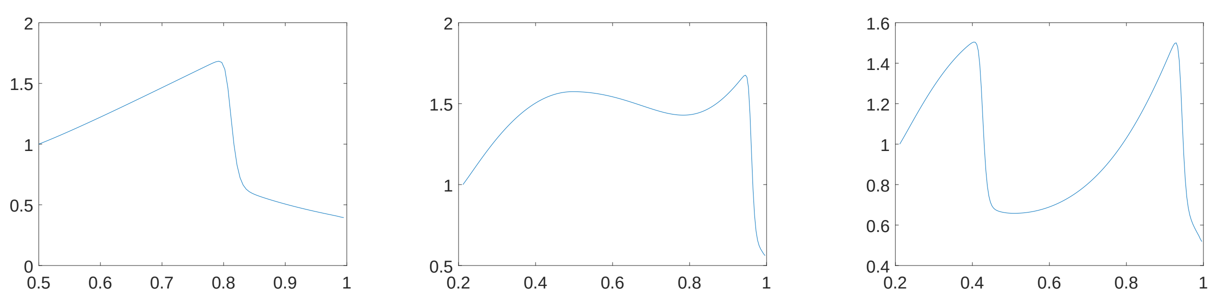

(a) (b) (c)

Figure 9: Mach number results solved with full Euler equations ($\gamma = 1.4$) and time-stepping for (9a) converging-diverging nozzle, (9b) two throat nozzle with one shock, and (9c) two throat nozzle with two shocks (see reference [6])

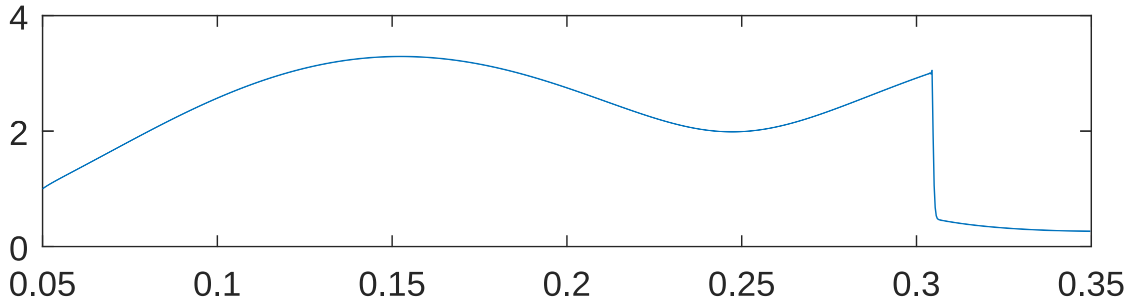

(a)

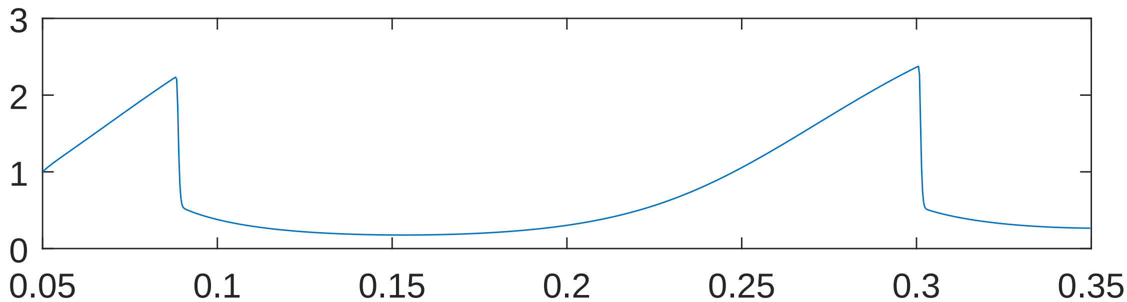

(b)

Figure 10: Non-unique solutions (Mach number) for a two-throat nozzle solved using full Euler ($\gamma = 1.4$) with shock-capturing and time-stepping to convergence (see ref [7]).

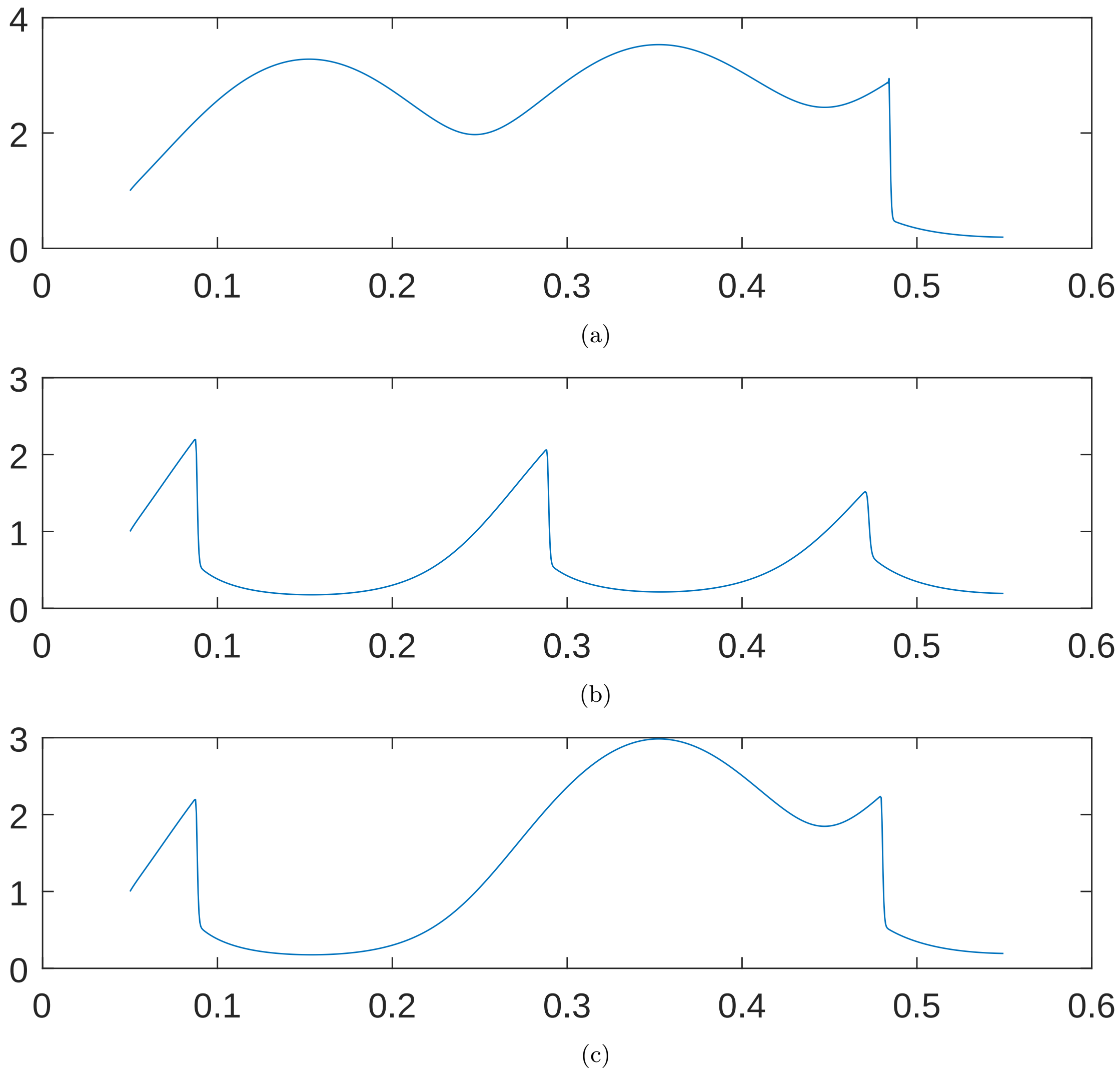

Figure 11: Non-unique solutions (Mach number) for a three-throat nozzle solved using full Euler ($\gamma = 1.4$) with shock-capturing and time-stepping to convergence(see ref. [7]).

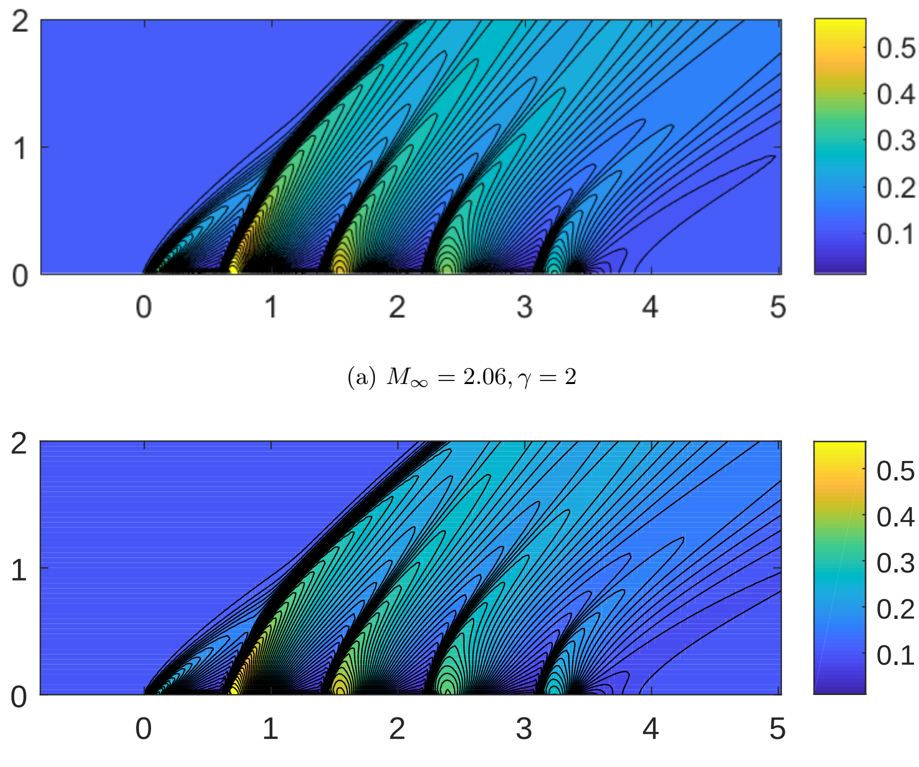

(a) $M_\infty = 2.06, \gamma = 2$

(b) $M_\infty = 2.26, \gamma = 2$

Figure 12: Numerical solutions for flow over wavy wall corresponding to water table results.

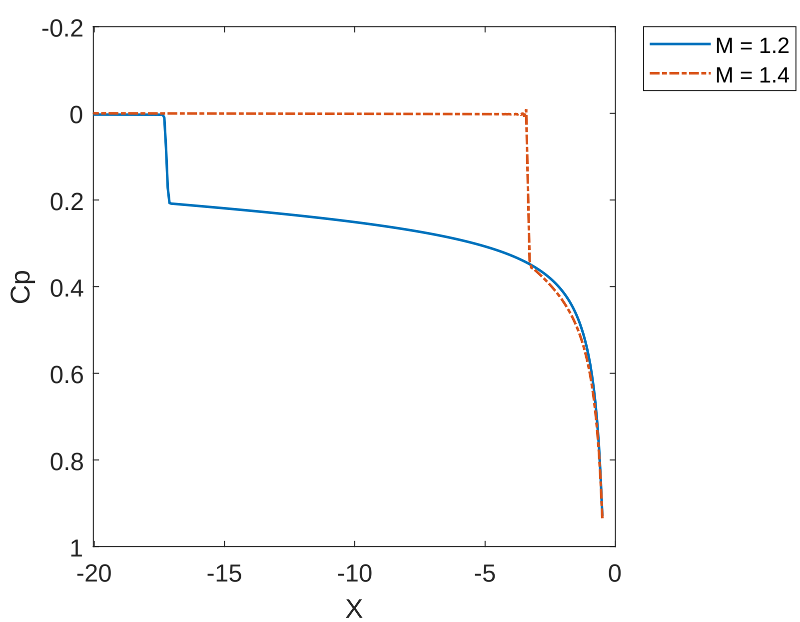

Figure 13: Bow shock locations of the cylinder in supersonic flow ($\gamma = 2$).

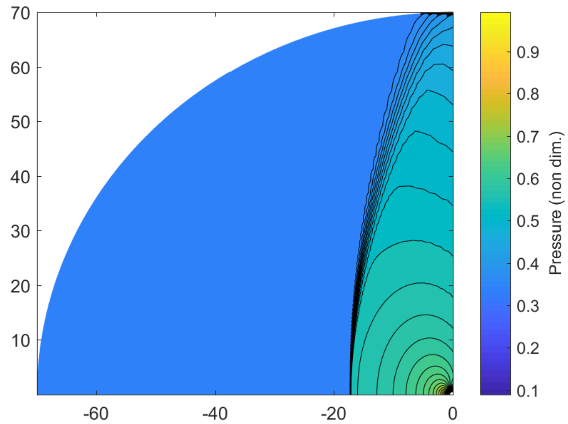

(a) $M_\infty = 1.2$

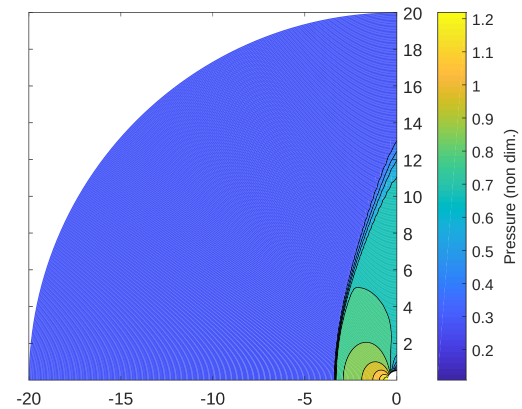

(b) $M_\infty = 1.4$

Figure 14: Numerical solutions of isentropic Euler equations ($\gamma = 2$) for supersonic flow over a cylinder.

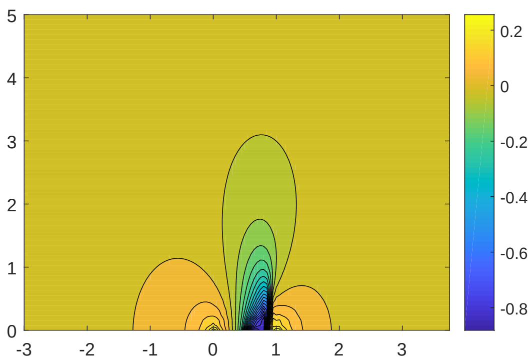

(a) Transonic Small Disturbance, $\gamma = 2$

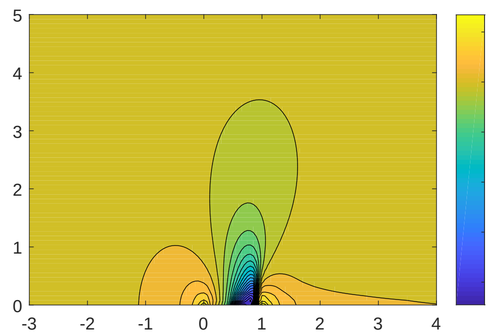

(b) Isentropic Euler, $\gamma = 2$

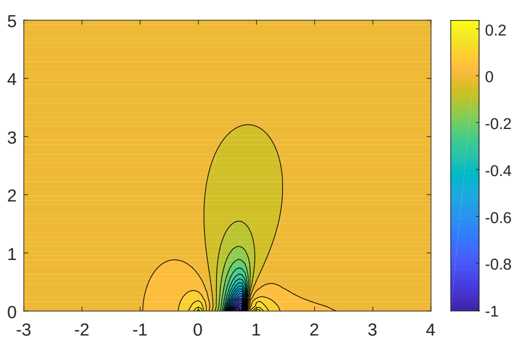

(c) Full Euler, $\gamma = 1.4$

Figure 15: Diamond airfoil in $M = 0.85$

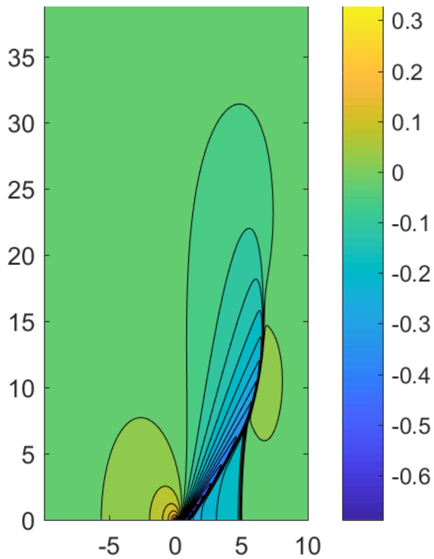

(a) Transonic Small Disturbance, $\gamma = 2$

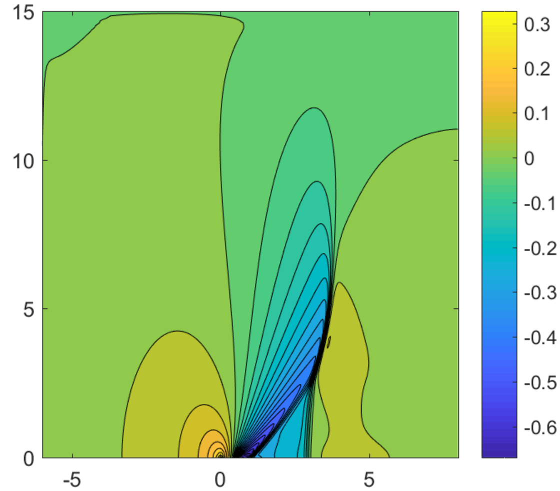

(b) Isentropic Euler, $\gamma = 2$

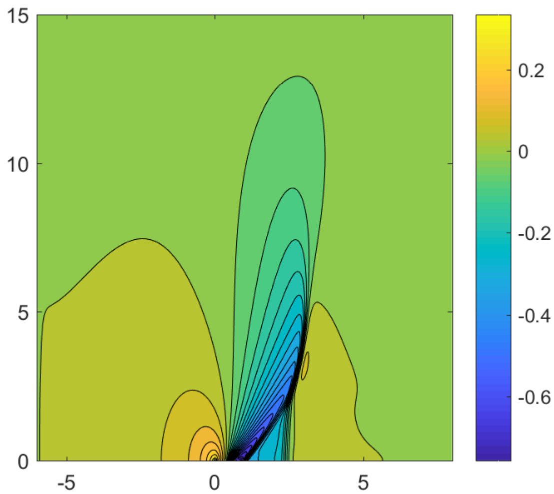

(c) Full Euler, $\gamma = 1.4$

Figure 16: Diamond airfoil in $M = 0.95$

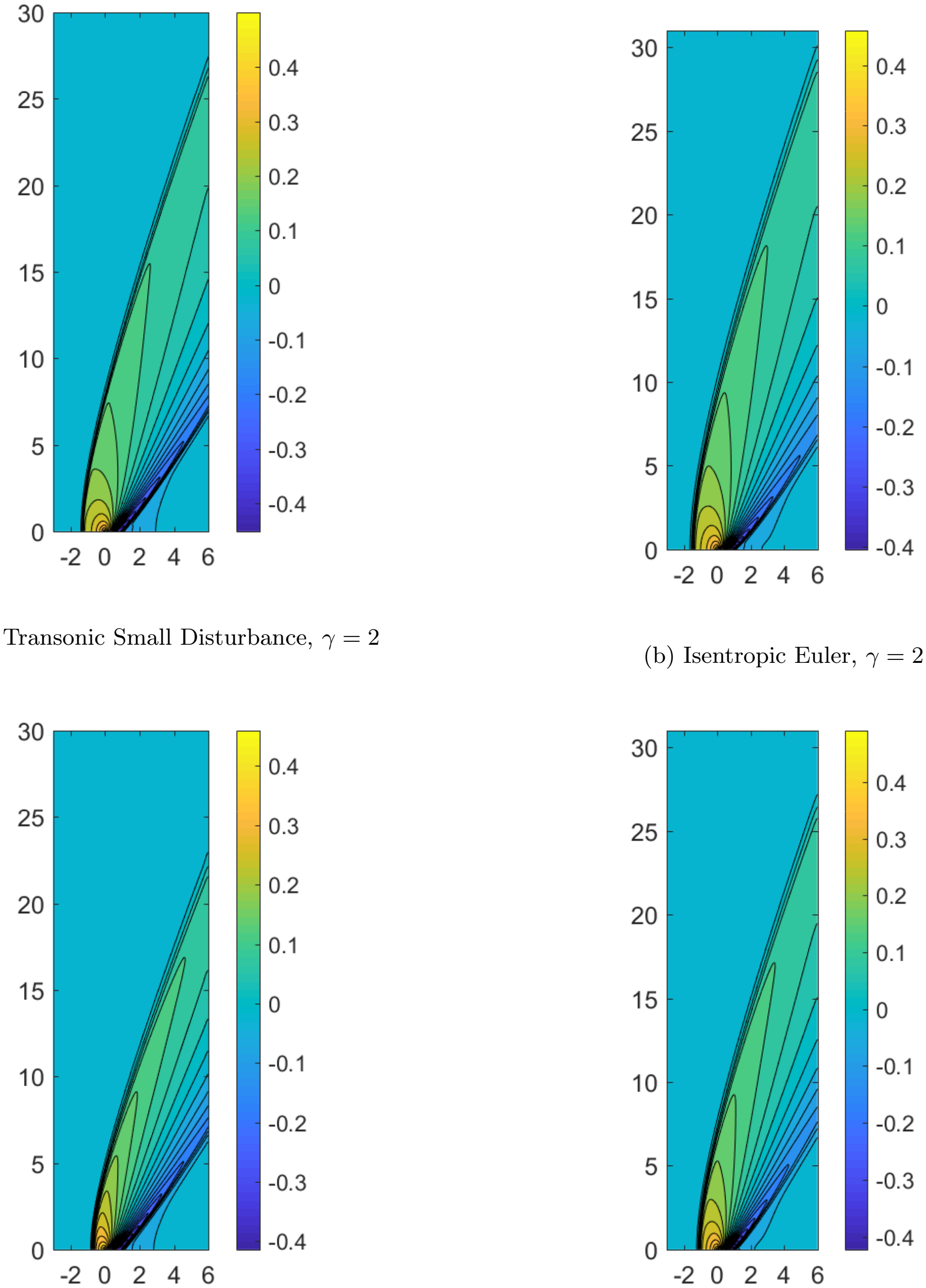

(a) Transonic Small Disturbance, $\gamma = 2$

(b) Isentropic Euler, $\gamma = 2$

(c) Full Potential, $\gamma = 2$

(d) Full Euler, $\gamma = 1.4$

Figure 17: Diamond airfoil in $M = 1.1$

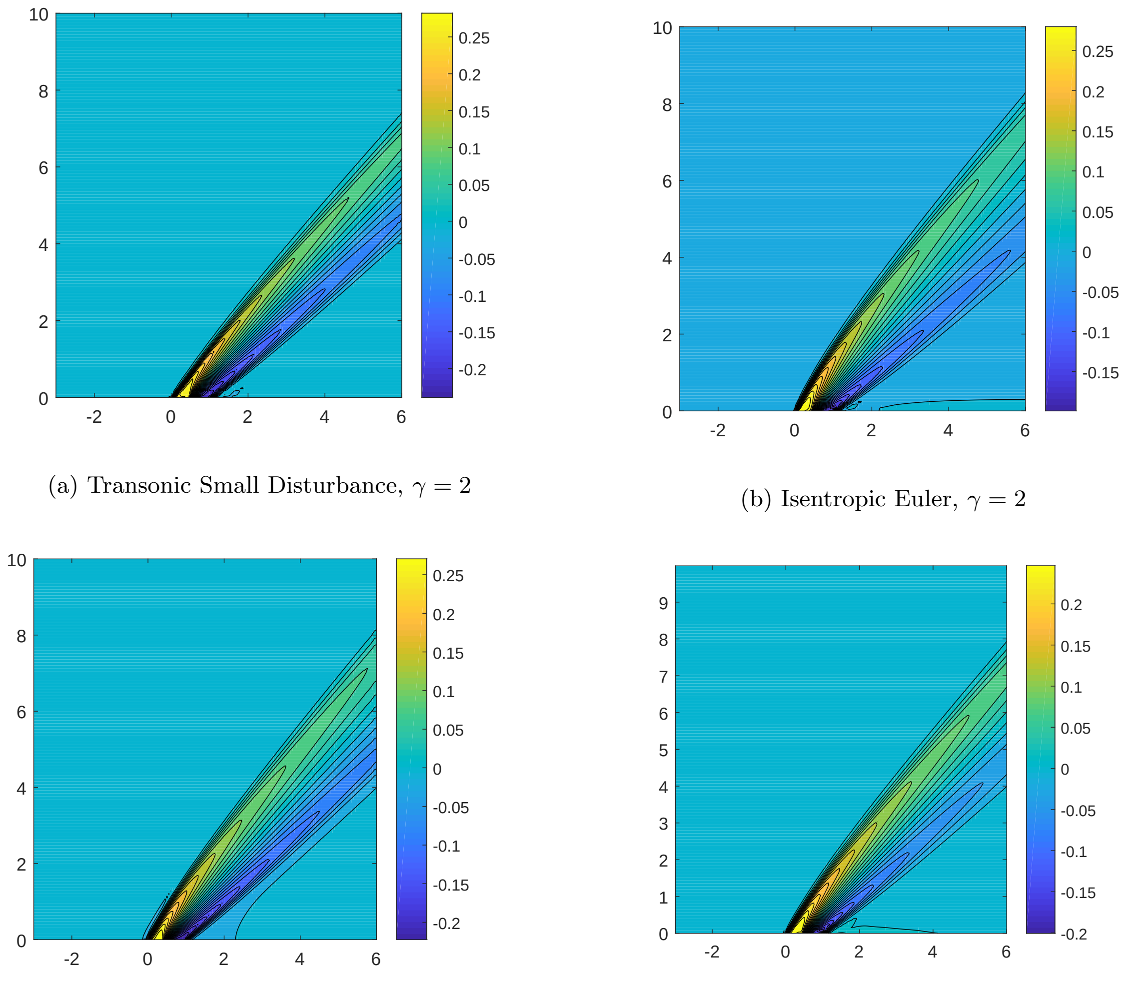

(a) Transonic Small Disturbance, $\gamma = 2$

(b) Isentropic Euler, $\gamma = 2$

(c) Full Potential, $\gamma = 2$

(d) Full Euler, $\gamma = 1.4$

Figure 18: Diamond airfoil in $M = 1.4$

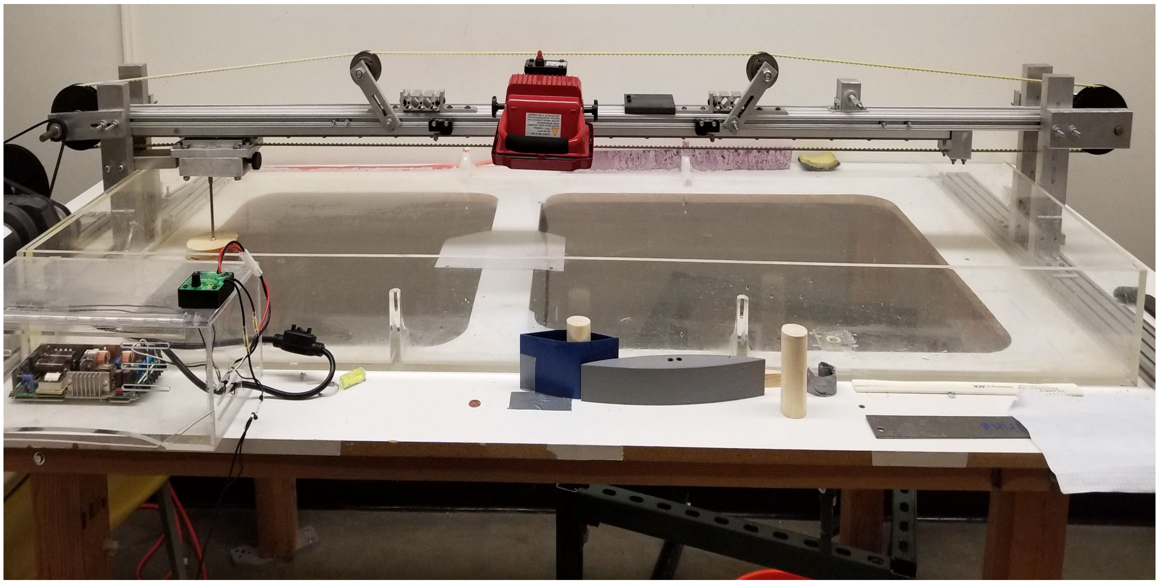

Figure 19: Water table testing apparatus

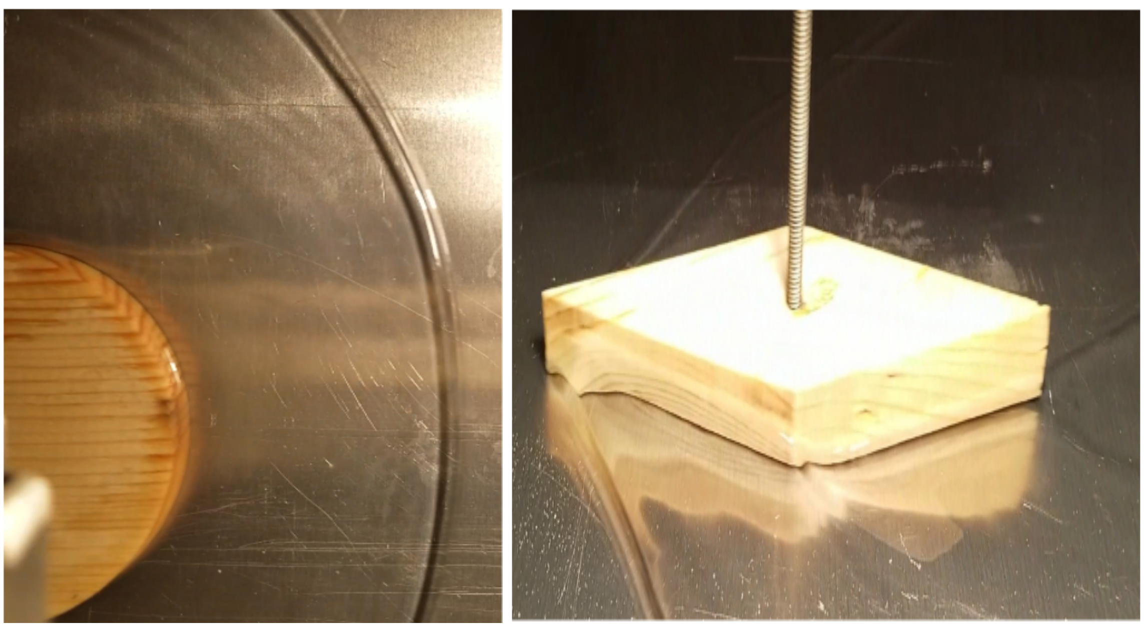

(a) (b)

Figure 20: Cylindrical and diamond airfoil on the water table

(a) Wavy wall

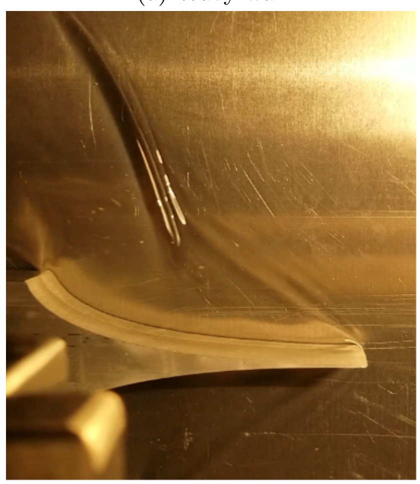

(b) Concave wall

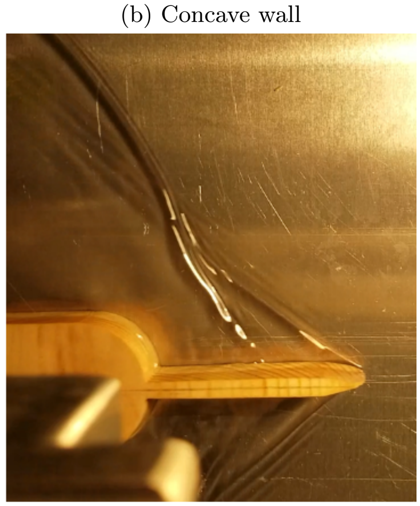

(c) Cylinder with spike

Figure 21: Experimental results of various model geometries

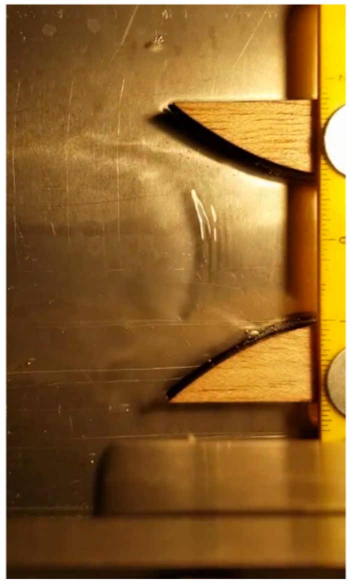

Figure 22: Experimental results of converging-diverging nozzle

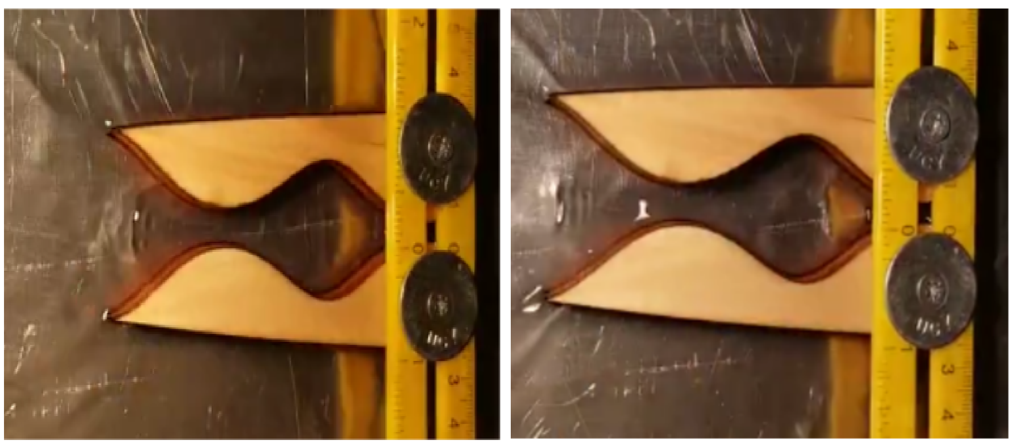

(a) Single Shock (b) Double Shock

Figure 23: Experimental results of double throat nozzle

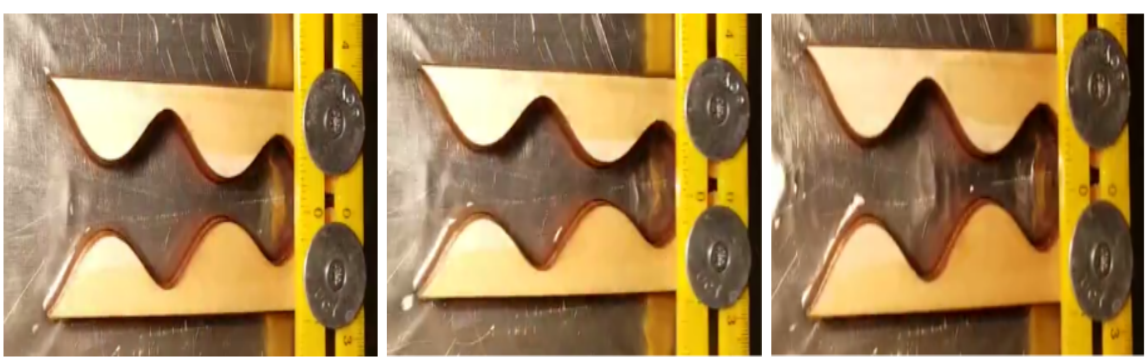

(a) Single Shock (b) Double Shock (c) Triple Shock

Figure 24: Experimental results of triple throat nozzle